ELSEVIER

Physics of the Earth and Planetary Interiors 120 (2000) 167–182

PHYSICS OF THE EARTH AND PLANETARY INTERIORS

www.elsevier.com/locate/pepi

Seismic emission activity of Earth's crust in Northern Kanto, Japan

Irina I. Tchebotareva [a,*], Alexiei V. Nikolaev [a], Haruo Sato [b]

[a] *Joint Institute of Physics of the Earth, Russian Academy of Sciences, B. Grusinskaya 10, Moscow, Russia*
[b] *Department of Geophysics, Graduate School of Science, Tohoku University, Aoba-ku, Sendai, Japan*

Received 1 January 1998; accepted 1 August 2000

Abstract

By using the semblance analysis of seismic noise prehistory of local earthquakes recorded by a dense seismic array, we reconstruct the image of distributed sources of weak seismic radiation beneath the Earth's surface. Array observations were carried out in the Nikko area, northern Kanto, Japan in 1993 by Joint Seismic Observation Team. The array consists of 195 three-component seismometers distributed along perpendicular profiles whose array diameters are 7 km. From the analysis of data, several active volumes in the upper crust were identified and new features of seismic emission discovered. A joint analysis of the coda and seismic noise shows that a mid-crustal magma body that was identified before by reflection analysis is both a scattering region and a source of seismic emission. Another large active volume is visible to the east of the array at depths of 2–15 km; it coincides with a known low-velocity and high-attenuation anomaly. This emission region corresponds to an area of large earthquakes.

Keywords: Crustal structure; Seismic emission; Emission tomography; Seismic noise

1. Introduction

Many geophysical processes in the Earth's interior are accompanied by radiation of seismic energy in a wide range of scales, from disastrous earthquakes to weak radiation that is a component of seismic noise. Earthquakes have attracted general attention from time immemorial due to their great significance for human life; however, the importance of seismic noise as a valuable source of information about the geodynamic state of the Earth was realized not so long ago. However, some interesting results were reported in the last century. In his book devoted to tides and associated phenomena, Darvin (1898) described observations of acoustic noise with a microphone in an underground vault. De Rossi, who was the author of this investigation, came to the conclusion that the observed noise was of terrestrial origin and remarked some peculiarities of the underground radiation.

One of the well-known types of endogenous radiation is volcanic tremor. It was discovered by Omori (1911) during the eruption of Usu Volcano, Japan; since that time many scientists have observed and studied similar phenomena on volcanoes all over the world. Volcanic tremor usually accompanies eruptions and is then radiated from sources near the

* Corresponding author.
E-mail address: chari@synapse.ru (I.I. Tchebotareva).

0031-9201/00/$ - see front matter
PII: S0031-9201(99)00163-6

bottom of the active crater, but occasionally it is recorded between eruptions and the source is situated at depths down to 30–60 km (Eaton, 1967). Different hypotheses for the mechanism of excitation of volcanic tremor exist (Sassa, 1935; Finch, 1949; Omer, 1950; Sakuma, 1957; Shima, 1960; Kubotera, 1974; Seidl et al., 1981; Tokarev, 1981; Cosentino et al., 1982; Gordeev, 1985) but none of these provides a full explanation of all features of this complex phenomenon.

Phenomena that can be explained by the existence of endogenous sources are not confined to volcanic regions. In the early 1950s, Gamburtsev (1960) called attention to a strange behavior of seismic noise (10–40 Hz) observed in Tadjikistan: the variation of amplitude was the same in value and simultaneous at two recording sites with a separation of 5 km and there was no correlation with wind. Gamburtsev proposed a deep origin for this seismic noise component.

The interest in the study of deep sources of seismic noise increased in the mid-1970s, when a systematic study of phenomena called seismic emission began. From the spectral analysis of teleseismic records, Zhadin (1971) found distinct high-frequency (>2 Hz) wave trains after the direct P-arrival. His interpretation was that the high-frequency components were excited in the Earth triggered by direct P-waves. Study of temporal variations of amplitude envelope of high-frequency noise (15–60 Hz) was carried out by using narrow-band high-gain instruments (Rykunov et al., 1979, 1980, 1982; Diakonov et al., 1990). These workers found a correlation between seismic noise level and low-frequency strain processes: tides, storm microseisms, and seismic waves from large distant earthquakes. They reported that the seismic emission activity of the Earth changes in time and space, exhibits a high sensitivity to stress and vibration, and a frequency selectivity to external forces. They also consider the possibility that seismic emission gives rise to fractal properties of seismic noise (Rykunov et al., 1986, 1987; Smirnov and Cherepantsev, 1991; Berdyev et al., 1992; Mukhamedov, 1992).

In spite of this great amount of work available at present, we should concede that the true nature of seismic emission is still not well-understood. Most researchers try to relate seismic emission to rock failure and the growth of defects under the variation of background stress field (by analogy with acoustic emission) or with restructuring of a multi-scale block structure in the presence of dry friction and volume fluctuations (Rykunov et al., 1979; Krylov et al., 1991; Mukhamedov, 1992). The Earth's crust is very heterogeneous both as regards geologic structure and rheology, as well as the distribution of structural stress. Hence, it is natural to expect that emission sources are non-uniformly distributed in space. Since almost all observations reported so far on seismic emission were carried out using a single receiver, it was difficult to locate a source of radiation and identify it in relation with real geological objects. Diakonov et al. (1989, 1990, 1991) found depths with a stable large amplitude of noise in the seismic (>1 Hz) and acoustic frequency ranges in both tectonically active and quiet areas. Detailed study of these phenomena showed that large amplitude noise occurs in crushed and cracked regions, faults and fracture zones. Some information on the spatial distribution of emission sources were found by borehole observations. Observations made in Belorussia with modern high-sensitive equipment for frequencies of 0.5 to 1000 Hz showed that seismic noise with large amplitude at some depth is evidently related to the emission activity at this depth (Belyakov and Nikolaev, 1995).

In these researches, the seismic emission phenomena were studied on the basis of amplitude information; a source of radiation was associated with a receiver on the surface or in boreholes. To clear up the details of mechanism of excitation of seismic emission, to monitor the dynamics of seismic sources, and to estimate the relative energy contribution of emission component into the global noise field of the Earth, it is first necessary to locate sources of radiation and compare them with real geophysical objects and fields. Several studies were made before to locate scattering sources from coda analysis in a deterministic framework (Key, 1967; Lynnes and Thorne, 1989; Hedlin et al., 1991). In these works, they estimate azimuthes and apparent distances of ''secondary'' sources. We made similar study with use of semblance analysis (Nikolaev and Troitskiy, 1987; Nikolaev et al., 1986). Our method permits to make three-dimensional source location, i.e., to estimate azimuths, apparent distances, and depths of

seismic sources. The first work was done by analyzing vertical-component records of noise and coda of teleseismic earthquakes obtained at the NORSAR array (Nikolaev and Troitskiy, 1987; Nikolaev et al., 1986). The method was also used for geothermal energy exploration by L.N. Ryknuov, B.M. Shoubik, and V.L. Kiselevich (Arnason and Flovenz, 1992). Here, we call our method, which focuses on the location of seismic emission points as ''emission tomography''. This name more clearly reflects the meaning of the method; as a result, we get three-dimensional images of the medium where the distribution of brightness shows the distribution of active volumes, in other words, we derive portraits of the medium in terms of its ability to produce or scatter seismic energy. In this paper, we describe the results of analysis of seismic noise data recorded in the Nikko-Ashio district near the volcanic front, Honshu, Japan. In contrast to our previous studies, we analyzed three-component records based on an extended version of emission tomography adapted for three-component data processing.

2. Data processing algorithm

Suppose that a small volume in the Earth radiates a weak seismic signal. This seismic signal has a very simple structure, in a homogeneous medium this being a spherical wave. In a real medium, the signal trajectory is distorted due to lateral velocity variation but a spatial signal coherence remains. This fact can be used for seismic source detection. To extract the spatially coherent component of seismic noise and reconstruct an image of the weak seismic source we use a coherency measure for multi-channel data named semblance (Taner and Neidel, 1971; Nikolaev and Troitskiy, 1987; Nikolaev et al., 1986, 1991):

$$S = \frac{\sum_{j=0}^{T}\left[\sum_{i=0}^{K} f_{ij}(\tau_i)\right]^2}{\sum_{j=0}^{T}\sum_{i=0}^{K} f_{ij}^2(\tau_i)}, \qquad (1)$$

where K is the number of channels, T is the time window length in samples, f_{ij} is the instantaneous amplitude of the j-th sample at the i-th recording site, τ_i is the time shift in the i-th channel appropriate to the path of a hypothetical signal from a focused grid point. Scanning the structure over a three-dimensional rectangular grid, we derive the spatial distribution of semblance coefficient that characterizes the emission and scattering properties of the Earth.

If there is no coherent component of seismic noise and only independent identically distributed Gaussian noise is present on each channel, the semblance has the β-distribution with expected mean and variance,

$$\langle S\rangle = 1 \qquad (2)$$

$$\sigma^2 = \frac{2}{T}\left(1 - \frac{1}{K}\right).$$

These formulas can be derived as follows. Semblance is connected with the F-statistic (Douze and Laster et al., 1979)

$$\frac{S}{K} = \frac{F}{F + K - 1}. \qquad (3)$$

In mathematical statistics the F-statistic is defined (Kramer, 1974) as

$$F = \frac{m}{n}\kappa, \qquad (4)$$

where n and m are degrees of freedom; $\kappa = \sum_{j=1}^{m}\xi_\nu / \sum_{j=1}^{n}\eta_\nu$, ξ_ν, η_ν are independent random variables distributed as $N(0, \sigma^2)$. According to Douze and Laster (1979), the degrees of freedom are $n = 2Bt = T$, $m = T(K-1)$; B is the bandwidth in Hz and t is the time window in seconds.

From Eqs. (3) and (4),

$$\frac{S}{K} = \frac{\kappa}{\kappa + 1}.$$

Hence, the statistics of (S/K)-measure is a β-statistic as defined in Kramer (1974), with the same degree of freedom as for the F-statistic. The sample moments of the β-statistic are given by

$$a_\nu = \frac{\Gamma\left(\frac{m}{2} + \nu\right)}{\Gamma\left(\frac{m}{2}\right)} \frac{\Gamma\left(\frac{m+n}{2} + \nu\right)}{\Gamma\frac{(m+n)}{2}}.$$

From this relation it is possible to calculate the first and second central moments of *S*-measure:

$$\langle S\rangle = Ka_1 = 1$$

$$\sigma^2 = a_2^2 - a_1^2 \approx \frac{2}{T}\left(1 - \frac{1}{K}\right).$$

The β-distribution is asymptotically normal (for $m,n > 30$), hence the 95% confidence band equals $2\sigma \approx \sqrt{(2/T)}$. That is, under the assumption that no signal is present, semblance maps have a uniform distribution of brightness, the statistical scatter of brightness in an image depending on the variance. With 95% probability the values of semblance fall in the band $[1 - 2\sqrt{(2/T)}, 1 + 2\sqrt{(2/T)}]$.

When coherent signals from an emission source are in the noise-like wave field, a bright spot appears in the reconstructed image. Semblance sharply increases for those grid points which are closer to the source. Semblance is a function of the signal-to-noise ratio. Let us assume for simplicity that an identical signal is present on each channel, E_s and E_n are signal and noise power on each channel. It is possible to verify that

$$\langle S\rangle = \frac{KE_s + E_n}{E_s + E_n} = 1 + \frac{(K-1)E_s}{E_s + E_n}.$$

For a weak signal and $K \gg 1$,

$$\langle S\rangle \approx 1 + K(E_s/E_n). \tag{5}$$

The use of a three-component receiver allows a significant improvement in the method of emission tomography. Namely, instead of the f_{ij} in Eq. (1) we can use a simple projection of three-component particle motion on the direction of oscillation for a selected type of wave: compressional wave (P) and two components of shear wave (SV and SH) in the far-field zone appropriate to a given ray.

Numerical simulation and analysis of real data has shown that the use of three-component data improves the quality of images. It is possible to make use energy in the appropriate type of wave and to filter out waves with different coherent polarizations. We have no special difficulties in the choice of projection direction for the analysis of compressional waves, but difficulties arise in the choice of projection direction for the transverse components of seismic waves. For shear waves, we take the projection in a plane perpendicular to the ray direction. When reconstructing images in shear waves we used a modification of the coherent semblance measure as

$$\tilde{S} = \frac{1}{2}\sum_{j=0}^{T}\left[\frac{\sum_{i=0}^{K} f_{ij}^{\mathrm{SH}(\tau_i)}}{\sqrt{\sum_{j=0}^{T}\sum_{i=0}^{K}\left[f_{ij}^{\mathrm{SH}}(\tau_i)\right]^2}} + \frac{\sum_{i=0}^{K} f_{ij}^{\mathrm{SV}}(\tau_i)}{\sqrt{\sum_{j=0}^{T}\sum_{i=0}^{K}\left[f_{ij}^{\mathrm{SV}}(\tau_i)\right]^2}}\right]^2, \tag{6}$$

where f^{SH} and f^{SV} are projections of instantaneous amplitude in the SH and SV directions, the other notation being similar to that in Eq. (1).

In the absence of a specific dominant source, ''random noise... is composed of multiple wave types (surface and body) from multiple sources. An array of seismometers would exhibit low coherence both between components of motion at any site in the array and between the site'' (Carter et al., 1991). When different components of motion at a single station is uncorrelated and are identically distributed Gaussian noise, it is possible to show that the $\tilde{S}$-measure has an asymptotically normal distribution with mean and variance:

$$\langle \tilde{S}\rangle = 1, \tag{7}$$

$$\tilde{\sigma}^2 = \frac{2}{T}.$$

These formulas for $\tilde{S}$-measure coincide with the respective formulas (Eq. (2)) for the *S*-measure. A high semblance value, $\tilde{S} \geq 1 + 2\tilde{\sigma}^{2\prime}$, indicates that a coherent arrival presents in the noise.

To derive Eq. (7) we rewrite Eq. (6) as

$$\tilde{S} = \left(\frac{1}{T}\right)\sum_{j=1}^{T}\xi_j^2,$$

where

$$\xi_j = \left(\frac{1}{2K}\right)\sum_{i=1}^{2K} u_{ij}\sqrt{(2K)},$$

$$u_{ij} = \begin{cases} \dfrac{f_{ij}^{\mathrm{SH}}\sqrt{(KT)}}{\sqrt{\sum_{j=0}^{T}\sum_{i=0}^{K}\left[f_{ij}^{\mathrm{SH}}\right]^2}}, i = 1,K \\ \dfrac{f_{ij}^{\mathrm{SV}}\sqrt{(KT)}}{\sqrt{\sum_{j=0}^{T}\sum_{i=0}^{K}\left[f_{ij}^{\mathrm{SV}}\right]^2}}, i = K+1,2K \end{cases}.$$

If records on channels are not correlated and consist of random noise with zero mean and identical variances, the u_{ij} obeys a Student's *t*-distribution. Consequently, u_{ij} are asymptotically normal with mean 0 and variance 1. Hence, ξ_j is also asymptotically normal, being the means of normally distributed variables; the mean of ξ_j is 0 and the variance is

$$\sigma_\xi^2 = \frac{\sigma_u^2}{n} = \frac{\left(\sqrt{(2k)}\right)^2}{2K} = 1.$$

Therefore, $\tilde{S}$ follows the χ^2-distribution with T degrees of freedom, which is also asymptotically normal. By virtue of a normalization, the mean and variance of $\tilde{S}$ are described by Eq. (7).

It is necessary to make one important note. In the above data processing description it was supposed that the polarizations of compressional waves coincide with the directions of approach of waves at a recording site and the polarizations of shear waves is in the plane are orthogonal to the ray. Such approximations are adequate when the sensors are installed in boreholes. Nevertheless, in our case the observations were carried out at the free surface where reflection and conversion strongly depend on angle of incidence. Therefore, the real polarization of a compressional wave can deviate appreciably in some cases from the ray direction. To make single-station corrections, it is necessary to have exact information on the topography at each recording site and a very good three-dimensional velocity model of the medium for exact tracing of seismic rays. It is clear that this task is difficult. The results of our study show that the use of a simplified data processing technique (half-space with no topography), even though a crude one, works well even for surface recording and allows us to locate deep-seated emission sources.

3. Data

In our research the data of seismological observations carried out by ''The 1993 Joint Seismic Observation Group in and around the Nikko Area'' is used. The geometry of the dense seismic Nikko array deployed in northern Kanto, Honshu is shown in Fig. 1. The Nikko array, which consists of 195 three-component seismic stations, covered an area of 7×7 km with average spacing of 70 m. The seismometers were mostly installed on bedrock or on artificial concrete foundations, some partly being buried in soil. They were installed in the mountains at heights of 650–1300 m above sea level, in an area with low cultural and traffic noise. We used the frequency band 4.5–50 Hz.

It is necessary to note that the observational arrangement used has serious disadvantages as to the

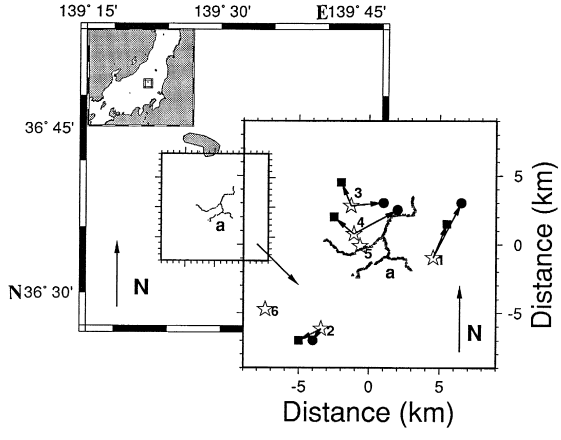

Fig. 1. Nikko-Ashio area, Honshu, Japan. Configuration of the seismic array and the images of the hypocenters of earthquakes 1–6 in Table 1 (a) Array geometry, open stars are earthquake epicenters according to the catalog; the black squares are source images from P-waves; black circles are source images from S-waves.

application of the method of emission tomography: the areal distribution of sensors is essentially non-uniform and is controlled by the road geometry where it was possible to transport the equipment in a mountainous area and the wave front is distorted due to the rough topography and velocity heterogeneities along a ray-path. The latter effect is especially strong at high frequencies. Besides, in our deployment we had very short samples of microseismic noise because recording was made in the triggered regime with 4-s pre-event noise. We used these 4-s noise samples ahead of the P-onset for our analysis. Nevertheless, despite such serious disadvantages, we could reconstruct a clear image of a deep emission source, which was supported by a series of positive factors. As already mentioned above, the network included a large number of three-component receivers, the initial material had excellent quality. The district, in which the seismic network was installed, is represented mostly by basaltic rocks. Velocity heterogeneities are probably not too strong and the influence of topography is not so destructive as to destroy correlation and polarization. Furthermore, rough topography and inaccessibility of this district have reduced cultural and traffic noise.

We analyzed the records of six local earthquakes with $M \sim 2.5–3$ and noise samples before the P-wave onsets. Information about these earthquakes is listed in Table 1. The sources of these earthquakes have similar focal depths (7–9 km) and are distributed around the Nikko seismic array as shown in Fig. 1. All records contain 20 s of data with a short noise prehistory. Fig. 2 shows example seismic traces. Time difference between direct P- and S-waves is about 1.5 s. The length of seismic noise samples ahead of the P-onset are about 4 s. For reconstruction of an image we use the first 3.6 s of each record. The time window for seismic noise is selected to be as long as possible but does not exceed the P-wave onset of the earthquake. When we make emission images for coda, we use last 12 s of records. When we reconstruct images of earthquake sources, time window for P-waves is 0.85 s (85 samples) and for S-waves is 1.00 s (100 samples); time windows start from the time of arrival. All time windows are shown in Fig. 2.

At the first stage of handling all records were subjected to visual analysis. Channels contaminated with noise and anomalous temporal shifts were rejected. The preliminary analysis of data has shown that amplitudes of seismic noise and coda of local earthquakes can differ for different array stations. There exist researches (Yoshimoto et al., 1993), which showed that for high-frequency oscillations it is impossible to neglect local influence of the medium. Site effects may be considerable even when registering equipment is installed on hard-rocks, especially on granite. To remove the influence of site effects from the final results, traces are reduced to zero average and normalized by using the mean square three-component amplitude.

In our study, the noise time series contains 360 samples (T). According to formulae (2) and (7), when no spatially coherent noise signal is present, we have maps of S and $\tilde{S}$ measures with

$$S = 1 \pm 2\sigma = 1 \pm 0.15. \quad (8)$$

Before data processing, we discarded records of stations with strong cultural noise, large distortion of

Table 1
Information about earthquakes which noise prehistory we used for analysis

	Number of earthquakes					
	1	2	3	4	5	6
Date	09/11/1993	11/11/1993	14/11/1993	17/11/1993	17/11/1993	18/11/1993
Time of origin (h–min in JMA)	17–42	03–19	07–46	00–39	14–46	02–10
Depth (km)	9.0	7.3	7.8	7.5	7.7	7.7
Longitude (°N)	36.625	36.578	36.658	36.640	36.632	36.591
Latitude (°E)	139.540	139.452	139.475	139.478	139.482	139.407
Number of stations before rejection	147	165	159	153	169	174
Number of stations after rejection	101	100	85	101	93	109

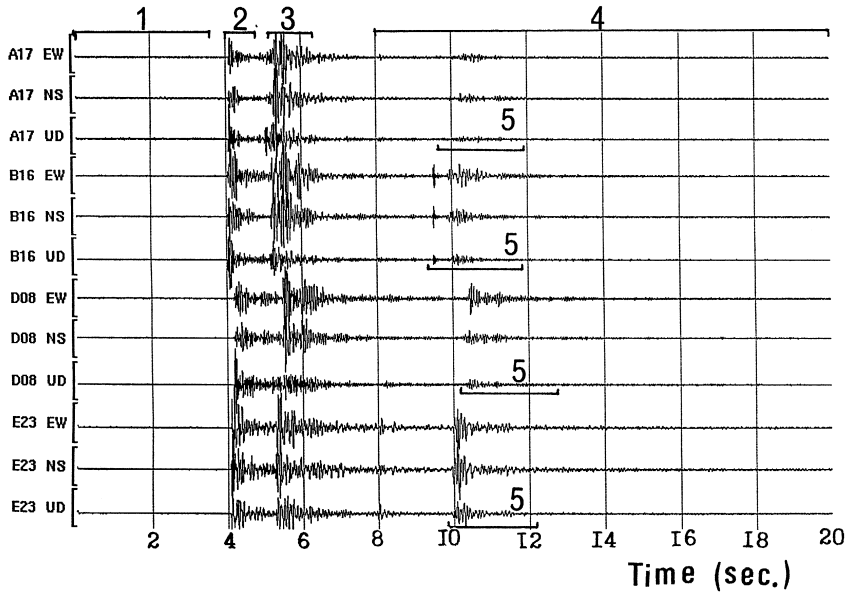

Fig. 2. Sample velocity seismograms of local earthquake 3 from Table 1 for stations A17, B16, D08 and E23. Time window used for reconstruction of emission images: (1) for seismic noise, (2) for direct P-waves, (3) for direct S-waves, (4) for coda, and (5) for reflection phase from a magma body.

direct waves of earthquakes and different frequency response. For these reasons the number of stations used for the image reconstruction was about 100 (K), as listed in Table 1. Hence, in the presence of a spatially coherent component, according to formula (5), in the grid point coinciding with source position we will have

$$S \approx 1 \pm \lambda, \tag{9}$$

where λ is the average signal-to-noise ratio in percent.

When we draw emission images we plot maps of $(S-1)$ and $(\tilde{S}-1)$ and a scale of brightness. For the grid points different from the emission source position the brightness of an image lies within the confidence band set equal to ± 0.15. Bright spots with brightness larger than 0.15 are significant with 95% probability. A signal-to-noise ratio of the energy radiated by an elementary volume equals the brightness value.

We should make a small remark here. We use darker colors to draw the brighter regions in the emission images; our pictures look like negatives. Nevertheless, we use the word ''brightness''.

4. Results

Numerical simulations using the parameters of real field observations show that the images of a radiation point has a smaller size for higher frequencies. In Fig. 3, the contour plots a, b and c show the reconstructed images of a source of a harmonic signal at frequencies of 5, 10 and 20 Hz, respectively, in a horizontal and two vertical cross-sections through the source. When we make emission images, the origin of coordinates in the horizontal section coincides with the center of the Nikko array (latitude 36°38′, longitude 139°29.4′). The positive direction of the x-axis and y-axis coincide with east and north, respectively. The brightness of each grid point equals $(S-1)/(S_{\max}-1)$, where $S_{\max}$ is the greatest semblance value at the grid point coincident with the source position. The source is placed beneath the center of array ($x = 0$ km, $y = 0$ km) at depth $h = 8$ km.

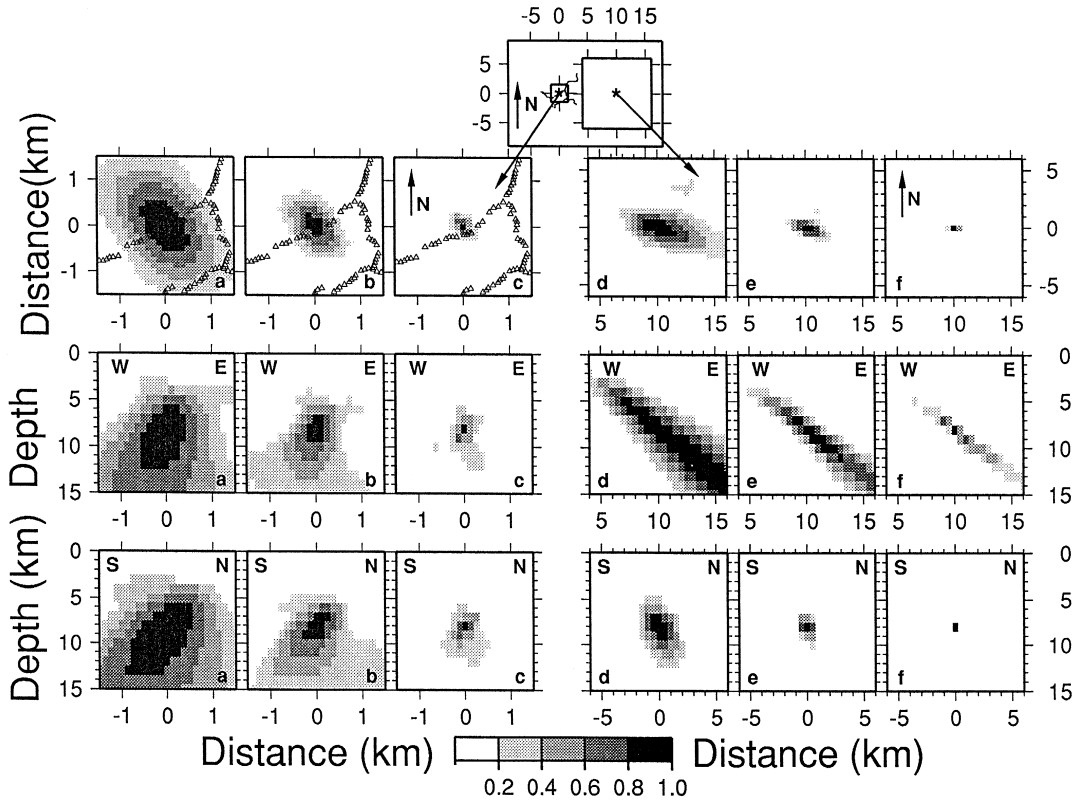

Fig. 3. Results of numerical simulation. Images of a point source at 8 km depth for horizontal and two vertical sections. Left-hand side shows results for a source beneath the array center ($x = 0$ km, $y = 0$ km) radiating signals with frequency (a) 5, (b) 10, and (c) 20 Hz. Right-hand side shows results for a source east of the array center ($x = 10$ km, $y = 0$ km) radiating signals with frequency (d) 5, (e) 10, and (f) 20 Hz. The density scale shows the normalized value of semblance: $(S-1)/(S_{max}-1)$, where S_{max} is the greatest semblance value at the grid point coincident with the source position.

The image is somewhat asymmetric in consequence of the asymmetry of the array geometry. The horizontal spatial resolution is several times better than the vertical. The maximum extent of a spot with brightness greater than 20% equals 1.2, 0.5, 0.125 km in the horizontal direction, and 7, 3, and 1 km in the vertical direction for frequencies 5, 10, and 20 Hz, respectively. In order to reliably restore a small high-frequency source, it is necessary to select a dense grid. However, reduction of grid spacing increases computer time in a square-law. For image reconstruction we have selected a compromise value of grid spacing: 0.5 km horizontally and 1 km vertically. This grid density is sufficient for reliable detection of sources with signal frequency up to 20 Hz, but is less reliable for the highest frequencies: we can miss a small radiating region that happen to occur on the edge of a bright spot. In the latter case, we underestimate the brightness of the emission source.

For all records we calculate images for radial and transverse components of seismic waves for depths 1–15 km with a step of 1 km over depth and in a 12×12 km square with a grid spacing of 0.5 km. Then, for more precise determination, for some samples the images were re-calculated over larger areas.

When a seismic source moves away from the center of the seismic array, the spatial resolution in the ''source–receiver'' direction becomes worse. That is, the ''bright spot'' is elongated in the source–receiver direction. Fig. 3d, e and f, shows images of a harmonic point source placed at depth of 8 km east of the array center ($x = 10$ km, $y = 0$ km) for frequencies 5, 10, and 20 Hz, respectively. A

comparison of contour plots a, b, c and plots d, e, f in Fig. 3 shows that the spatial resolution in the source–receiver direction becomes several times worse when the distance between the source and the array center approximately equals one and a half array diameters. Nevertheless, the resolution in perpendicular direction does not vary as much with source position. This means that for near-surface remote sources we shall receive ''spread shadows'' in the horizontal direction but a good resolution in depth. For deep remote emitters we shall get good resolution in the horizontal plane, but ''spreading'' over depth. This effect of ''spreading'' is observed for real data when we make emission images over a large area and for large depths.

4.1. Image of earthquake sources

In our study we used a two-layer model with $\nu_p = 5.2$ km/s and $\nu_s = 3.06$ km/s for depths down to 1.6 km and $\nu_p = 5.9$ km/s and $\nu_s = 3.47$ km/s for large depths according to Sakai (1994). The chosen velocity model is rather crude. To evaluate qualitatively the robustness of the velocity model, we show in Fig. 1 spatial differences between the locations of earthquake sources derived in two ways: source location estimated by means of P and S emission tomography and earthquake hypocenters determined from observations of a regional network as listed in Table 1. For regional location $\nu_p = 5.4$ km/s at $D = 0$–7.2 km/s at $D = 31$ km (depth dependence of velocity is linear), ν_s: 3.15 km/s at $D = 0$ km and 4.2 km/s at $D = 31$ km (depth dependence of velocity is linear). The accuracy of the routine procedure is only a few kilometers. The accuracy of the semblance location for homogeneous medium is better but open to influence of boundaries and local velocity inhomogeneities that can decline seismic ray.

Fig. 4 presents examples of source images for earthquakes 2 and 3 in P- and S-waves. In Fig. 4 we plot distributions of $(S-1)/(S_{max}-1)$ for P-waves and $(\tilde{S}-1)/(\tilde{S}_{max}-1)$ for S-waves. The time window for P-waves is 0.85 s (85 samples) with origin at P-onset; that for S-waves is 1.00 s (100 samples) with origin at S-onset. For an isotropic medium, when we make an error in the estimation of average velocity, the location shift of images in both types of

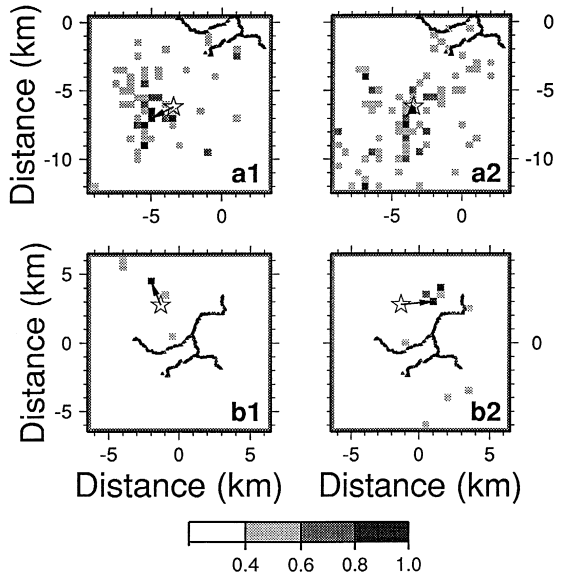

Fig. 4. Images of sources for direct waves: (a1) and (a2) earthquake 2 for P- and S-waves, respectively and (b1) and (b2) for earthquake 3 for P- and S-waves, respectively. Time window is 0.85 s for P-waves and 1.00 s for S-waves. The density scale shows the same as mentioned in the caption of Fig. 3.

waves should happen in the direction of source to array center. For compressional waves, this condition is fulfilled rather well (see Fig. 1). The horizontal and vertical displacement is 1–2 km, which agrees well with the routine procedure accuracy. However, the systematic outward location shift shows that the average velocity of a selected model is somewhat underestimated.

From a comparison of images of earthquakes in the southeastern part of the volume and in the central and northwestern part, we conclude that the medium to the east and to the south from the Nikko array is more heterogeneous. For earthquake 3, the images are well-localized as shown in Fig. 4b1 and b2. For earthquake 2, the main source image is enclosed by a large number of spots with lower brightness, creating a spatial aureole around the source image as shown in Fig. 4a1 and a2. This bright aureole appears to be due to scattering of the direct waves by surrounding small-scale heterogeneities.

From analysis of the images of earthquake hypocenters we can conclude that, when a biased velocity model is used the emission images of the medium will be slightly ''stretched'' in comparison

with the real situation. At a distance of about 6 km from the center of the array, the horizontal location shift will be about 1–3 km.

4.2. Image of the magma body

Previous seismic research revealed a mid-crustal velocity discontinuity near Shirane Volcano northwest of the Nikko array. It was interpreted as a thin crack filled with partially molten magma (Matsumoto and Hasegawa, 1996). It was estimated that this distinct reflector of S-waves is distributed over an area of 15×15 km in the depth range 8 to 15 km with a conical shape becoming shallow toward the summit of Shirane Volcano. It is well-known that records of local earthquakes recorded near this mid-

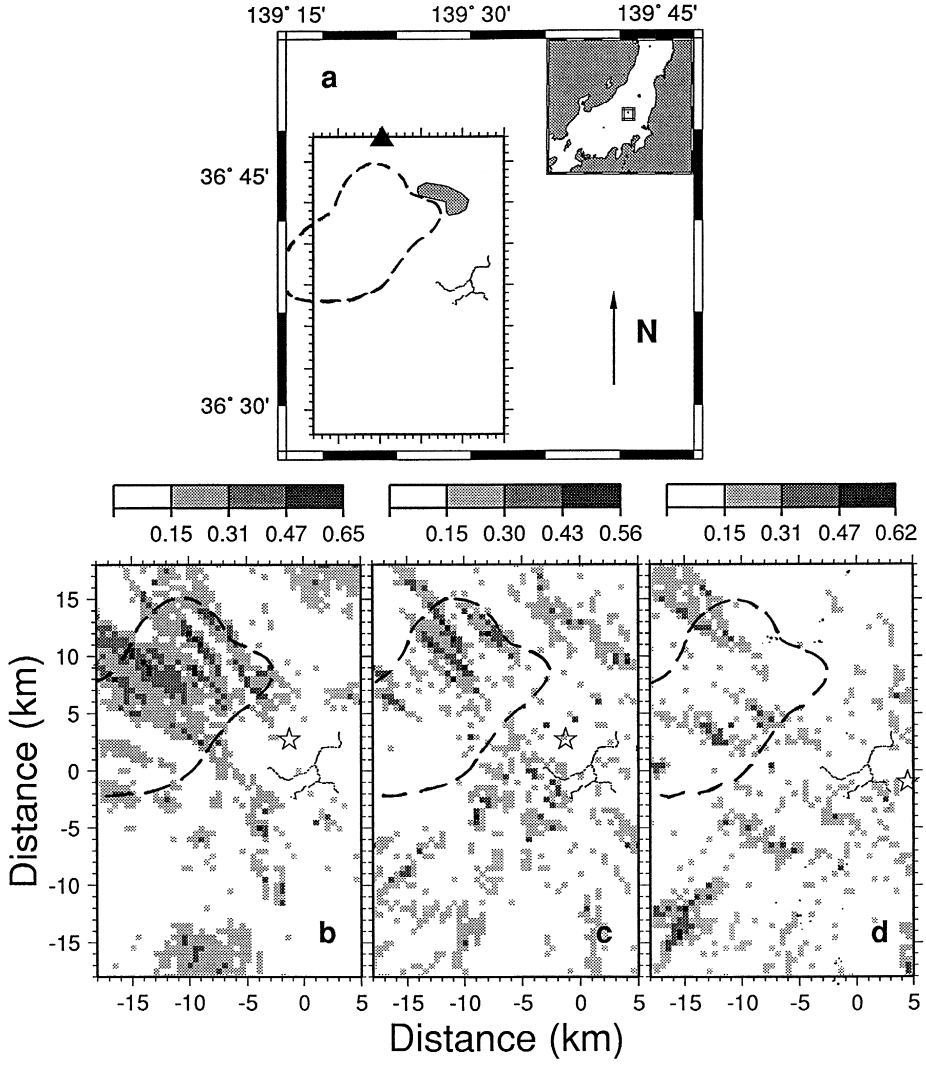

Fig. 5. (a) Location map of the Nikko array area. Black triangle is Shirane Volcano. Dashed line marks location of the mid-crust magma body according to Matsumoto and Hasegawa (1996). The large rectangle is a projection of the volume studied onto the horizontal plane. (b) and (c) are emission images of the medium at 9–11 km depth for radial and transverse components of reflection within coda, respectively, records of earthquake 3 being used. (d) is the emission image at the same depth for the transverse component of seismic noise, noise sample before P-onset of earthquake 1 being used. The density scale shows the value of $(S-1)$ for radial and $(\tilde{S}-1)$ for transverse components.

crust reflector contain easily identifiable S-to-S-reflected and S-to-P-converted one. Fig. 2 shows examples of records of local earthquakes; the distinct phase following the direct S-waves is clearly visible.

We use the reflected phases appearing in coda of local earthquakes to locate the reflector. We draw depth slices of brightness distributions which are the distributions of $(S-1)$ for the radial component of the coda and $(\tilde{S}-1)$ for the transverse component. For the radial component, we use a P-wave velocity model, for the transverse component an S-wave velocity model. We use the last 12 s of records that include clear-reflected phases. Fig. 5a shows the observational arrangement with the reflector location that was identified before from reflection analysis (Matsumoto and Hasegawa, 1996). Emission images at the depth of 10 km for radial and transverse components of the coda are shown in Fig. 5b and c. Emission images clearly show a bright scattering region to the northwest from the Nikko array that coincides with the position of the magma body. Fig. 5d shows an emission image for the seismic noise transverse component. From this picture, it is possible to see the bright region to the northwest from Nikko for noisy intervals. From a comparison of images b, c and d, it follows that the largest visible scattering and emission source correspond to the northern top of the magma body.

Emission radiation from northwest direction is observed for other noise samples but less intensive than for noise before earthquake 1. We conclude that intensity and composition of the weak emission sig-

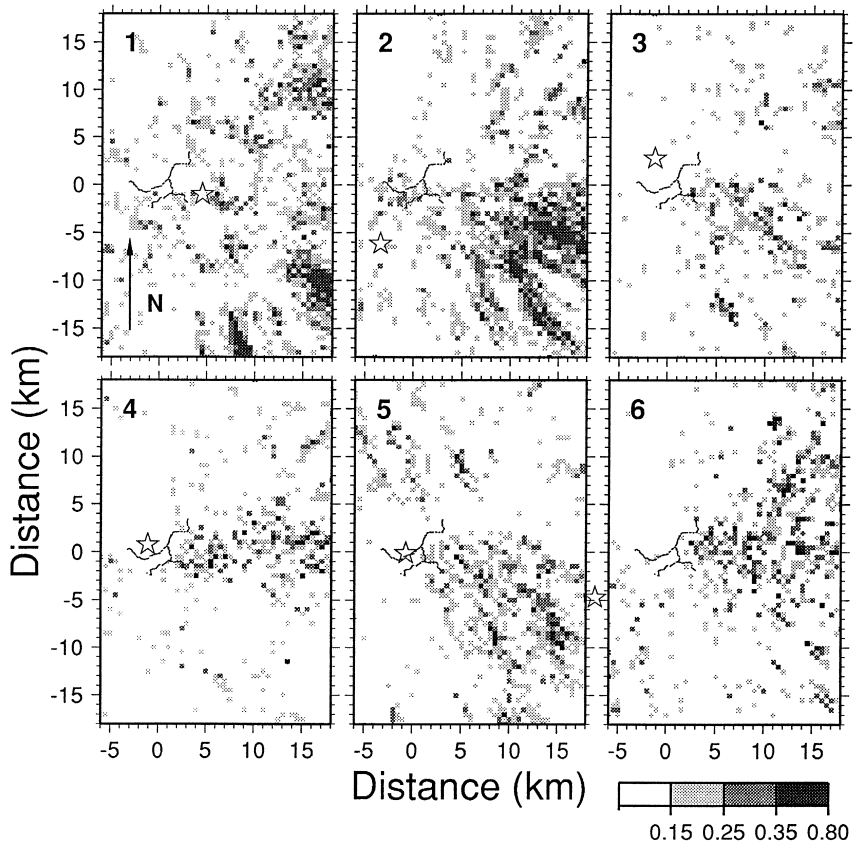

Fig. 6. Emission images of the medium at 11 km depth for the transverse component of seismic noise before the onset of P-wave for earthquakes 1–6 in Table 1. The density scale shows the same as mentioned in the caption of Fig. 5. Stars show the epicenters of earthquakes.

nal connected with magma body vary in time and for averaged image the deep northwestern source is brighter that surface ones (Tchebotareva et al., 1997).

4.3. Emission images of the medium

For seismic noise we made 12 three-dimensional images of the structure beneath the Nikko seismic array: six for compressional and six as shear. Similar to the previous section, we draw the horizontal section for different depth distributions of $(S-1)$ for the radial component of seismic noise and $(\tilde{S}-1)$ for the transverse component. For the radial component, we used the P-wave velocity model, for the transverse component the S-wave velocity model. It follows from Eqs. (8) and (9) that spots with brightness greater than 0.15 are significant with 95% probability and brightness value equals the signal-to-noise ratio (in percent) of seismic emission signal radiated by an elementary volume of $0.5 \times 0.5 \times 0.5$ km.

For all noise samples, a number of significant bright areas are observed where the value of the measures $(S-1)$ and $(\tilde{S}-1)$ are several times the confidence interval for uncorrelated noise. The maximum of $(S-1)$ and $(\tilde{S}-1)$ reaches 0.85 with confidence interval 0.15. It corresponds to signal-to-noise ratio of emission radiation from the elementary equal to $0.85\% = 0.0085$.

For depths of 0–2 km the images based on different noise samples differ, which is probably due to the influence of numerous surface sources whose intensity and space distribution vary rapidly in time. Down from depths of 2–3 km a stable feature for all noise samples begins to develop for shear waves: in the eastern and southeastern part a bright region appears which can be traced down to 15 km depth. The images for the transverse component of seismic noise before six earthquakes at the 11-km depth are plotted in Fig. 6. Fig. 7 shows the location of the studied volume. Fig. 7 shows time-averaged emission images for the transverse component of a seismic noise at the 11-km depth: the brightness in each point of the ''averaged image'' is the average of values of $(\tilde{S}-1)$ of six images in Fig. 6, in corresponding points. Fig. 8 shows emission images for the transverse component of seismic noise preceding event 4 at different depths. Two bright regions are well-traced over depths: the first one is in the central part from 2 to 15 km and the second one is in the eastern side from 6 to 15 km.

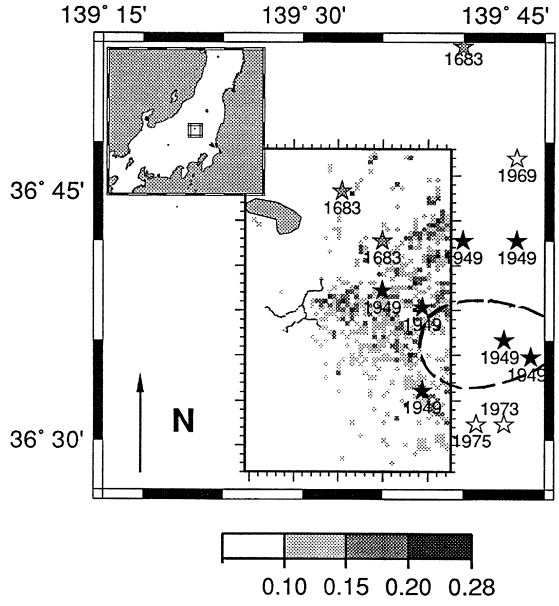

Fig. 7. Map of area of observation. Large rectangle encloses emission images. The emission image averaged over six images for transverse noise component at 11-km depth is shown in the figure. Stars are hypocenters of large ($M = 5$–7) historical and recent earthquakes from JMA catalog: black stars are 0–10 km in depth, gray stars are older earthquakes, open stars are 100–130 km in depth. A dashed curve shows the location of the low-velocity and large-attenuation anomaly according to Tsumura (1994) and Matsumoto (1996). The density scale shows the value of $(\tilde{S}-1)$ averaged over six corresponding values for different noise samples.

4.4. Spectra of emission radiation

From the above results, it follows that the emission component of seismic noise can be detected and the source of this weak seismic radiation can be located. It is possible to exploit this deep-generated seismic component as a source of useful information on global geodynamic processes in the Earth's crust. In this case, one would undoubtedly be interested not only in the distribution of bright emission volumes in the medium and their migration with time but also in the frequency spectra of seismic emission. The short time series that are at our disposal do not allow precise spectral resolution and an image based on short noise samples is indistinct. For spectral analy-

sis, we selected a noise sample before the P-onset of earthquake 2, with the hypocenter southwest of the Nikko array. For this sample, the emission radiation in both compressional and shear waves is the most intensive.

To estimate the emission spectrum the coherent beam-forming method is used. We first focus the Nikko sensors to amplify the signals coming from the chosen bright elementary volume. That is, we calculate the delay time for each receiver and stack traces with appropriate time shifts. Then we calculate the power spectrum of the coherent beam output. In this way, we calculate spectra for the radial and transverse components of noise using projections of noise amplitude in the respective directions.

In Fig. 9b, the characteristic power spectra for transverse components of noise for deep emission sources are shown. The focused points are at the depths 10–13 km. For comparison the spectra of the emission radiation of near-surface sources focused at $H = 0$ km are shown in Fig. 9a. For shear waves the spectra of emission radiation for deep sources quickly falls off with frequency, the maximum radiation corresponding to the lower end of the frequency range, 5–12 Hz.

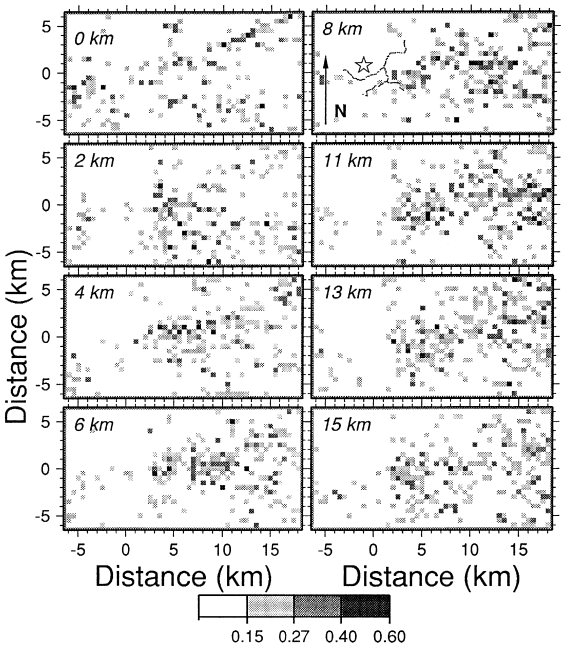

Fig. 8. Emission images of the medium at different depths for the transverse component of seismic noise before the onset of P-wave for earthquake 4. Depth is marked on each image. The density scale shows the same as mentioned in the caption of Fig. 5. Star shows the epicenter of earthquake 4.

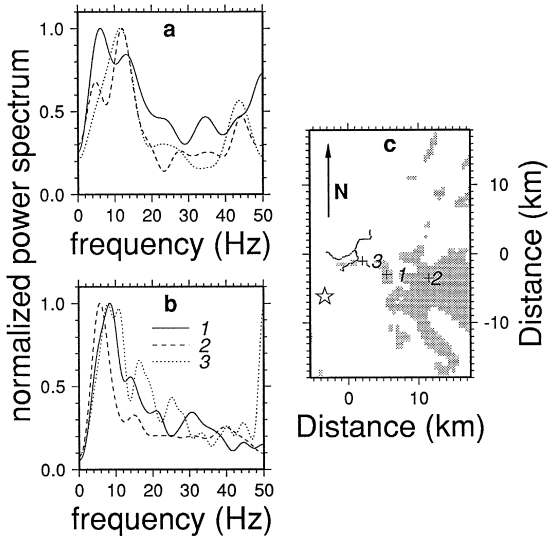

Fig. 9. Normalized power spectra of transverse component of seismic emission for noise samples before the onset of P-wave of earthquake 2: (a) for near-surface sources ($H = 0$ km), (b) for deep-seated sources (H = 10–13 km) within regions studied, (c) shows the location of active volume at 10–13 km depth, numbers 1–3 mark position of focused points and corresponds to numbers of curves on (b), respectively. Star shows the epicenter of earthquake 2.

5. Discussion and conclusions

Our study has confirmed existence of regions of weak seismic radiation in the Earth's crust. From comparison of emission images for the coda and seismic noise, we find a mid-crust reflector is also visible as a source of seismic noise. From our study of the distribution of surface sources for samples of seismic noise used here it follows that the deep source northwest of the Nikko array is brighter that surface ones (Tchebotareva et al., 1997). The conclusion therefore is that the deep bright region coinci-

dent with the position of the magma body is not a result of reflection of signals from a surface source. The magma body operates like an active source of emission that is related to processes that are in the magma body or near its surface.

Bright emission regions in the eastern part of emission images in Figs. 6 and 7 coincide with the area of large historical and recent earthquakes. From the results of a tomographic and seismic wave attenuation study of this region (Tsumura, 1994; Matsumoto, 1996), it is known that at the east of the array site, a region of low velocities (contrast up to 10%) and large attenuation of seismic waves ($Q_P^{-1} \sim 6*10^{-3}$ to $14*10^{-3}$) is localized in a range of depths of 0–10 km. On the surface, the low-velocity region corresponds to a sedimentary area. From our study, we estimate that this part of the medium is very heterogeneous. We find the images of earthquakes occurring to the south and east of the Nikko array have many additional small bright spots around the main image, due to reflection from near source heterogeneities (see Fig. 4). Low velocity and large attenuation also gives evidence of large heterogeneities in this volume. Therefore, it is possible to assume that the eastern part the volume studied is related to a very inhomogeneous, perhaps crushed and strongly fractured structure. The mechanism of excitation of emission radiation from this volume may be related to a restructuring of this heterogeneous structure under tectonic stress and to low-frequency deformation processes. In quantitative terms, one process of non-linear excitation of a high-frequency radiation by a low-frequency action during reorganization of a crushed structure in the presence of dry friction is described in Krylov et al. (1991). Coincidence of the active volume with the area of large earthquakes can be considered as a consequence of high tectonic activity in this area and the cause of large heterogeneity in this volume. As a rule, the hypocenters of large earthquakes are associated with faults, dividing rather large high-strength blocks. Nevertheless, from a map of distribution of horizontal strains (Geographical Survey Institute, 1987), it follows that in the eastern emission region the areal compressive strain dominates (-10^{-5} to $2*10^{-6}$). This situation promotes accumulation of shear stress even in a region with a low-strength structure that can generate large earthquakes.

Except emission regions coinciding with the magma body and the low-velocity anomaly, other bright regions were observed on the emission images; for example, as seen in Fig. 5d, at the southwest of the array. Further research is necessary for reliable identification of these emission sources.

Observations which we used for our analysis were unfortunately not originally intended for a study of seismic noise: the noise time series were very short with duration of 4 s. Nevertheless, even from an analysis of these short noise series, it follows that the method of emission tomography is a promising line of research. This method permits reconstructing the distribution of weak emission sources in the Earth and to monitor time variation and spectra. Our research, like some other recent seismic noise studies, shows that the noise may be considered an ''indicator'' of the state of the medium. At least seismic noise contains information on weak seismic emission whose time variation depends on the variation of the background stress field and on various internal and external geophysical processes.

Acknowledgements

The experimental data were provided by the 1993 Joint Seismic Observation Group in and around the Nikko area, as a cooperative usage of data at the Earthquake Research Institute, University of Tokyo. Special thanks to Professors Naoshi Hirata and Akira Hasegawa. We thank Katsuhiko Shiomi for his help in preliminary data selection, and to Dr. Oleg B. Khavroshkin for a helpful discussion. We thank Synapse Science Center/Moscow IRIS Data Center where data processing was made.

References

Arnason, K., Flovenz, O.G., 1992. Evalution of physical methods in geothermal exploration of rifted volcanic crust. Geotherm. Resour. Counc., Trans. 16, 207–214.

Belyakov, A.S., Nikolaev, A.V., 1995. Method of seismo-acoustic observations. Izv. Akad. Nauk Russ., Fiz. Zemli 8, 89–93, (in Russian).

Berdyev, A.A., Mukhamedov, V.A., Muradov, V.A., Seidov,

B.A., 1992. Anisotropy of high-frequency seismic noise during local earthquakes. Dokl. Akad. Nauk SSSR 322, 484–489, (in Russian).

Carter, J.A., Barstow, N., Pomeroy, P.W., Chael, E.P., Leahy, P.J., 1991. High-frequency seismic noise as a function of depth. Bull. Seismol. Soc. Am. 81, 1101–1114.

Cosentino, M., Lombardo, J., Patane, G., Schick, R., Sharp, A.D.L., 1982. Seismological research on Mt. Etna: state of art and recent trends. Mem. Soc. Geol. Inst. 23, 159–202.

Darvin, J.H., 1898. The Tides and Kindred Phenomena in the Solar System. Murray, London, 250 pp.

Diakonov, B.P., Karryev, B.S., Khavrishkin, O.B., Nikolaev, A.V., Rykunov, L.N., Seroglazove, R.R., Trojanov, A.K., Tsyplakov, V.V., 1990. Manifestation of Earth deformation processes by high-frequency seismic noise characteristics. Phys. Earth Planet. Inter. 63, 151–162.

Diakonov, B.P., Trojanov, A.K., Kuksonskii, O.A., Nazarov, A.N., Fadeev, V.A., 1991. Geology informativity of borehole study of high-frequency seismic noise. Volcanol. Seismol. 1, 112–116, (in Russian).

Diakonov, B.P., Trojanov, A.K., Nazarov, A.N., Fadeev, V.A., 1989. Seismo-acoustic noise at deep levels. Dokl. Akad. Nauk SSSR 309, 314–318, (in Russian).

Douze, E.J., Laster, S.J., 1979. Statistics of semblance. Geophysics 44, 1999–2003.

Eaton, J.P., 1967. Evidence of the source of magma in Hawaii from earthquakes, volcanic tremor and ground deformation. Trans. Am. Geophys. Union 48, 254.

Finch, R.H., 1949. Volcanic tremor. Bull. Seismol. Soc. Am. 39, 73–79.

Gamburtsev, G.A., 1960. Selected wokes. Akad. Nauk SSSR, Moscow, 424–425, (in Russian).

Geographical Survey Institute, 1987. In: Horizontal Strain in Japan 1985–1883. Geographical Survey Institute, Tsukuba, Japan, pp. 1–133.

Gordeev, E.I., 1985. The main properties of volcanic tremor of some Kamchatkan Volcanoes. Volcanol. Seismol. 3, 68–77, (in Russian).

Hedlin, M.A.H., Minster, J.B., Orcutt, J.A., 1991. Beam-stack imaging using a small aperture array. Geophys. Res. Lett. 18, 1771–1774.

Key, F.A., 1967. Signal-generated noise recorded at the Eskdalemuir Seismometer Array Station. Bull. Seismol. Soc. Am. 57, 27–37.

Kramer, G., 1974. Mathematical Methods in Statistics. Nauka, Moscow, 684 pp. (translated into Russian).

Krylov, A.L., Nikolaevskii, V.N., Ell, G.A., 1991. Mathematical model of nonlinear generation ultrasound by seismic noise. Dokl. Akad. Nauk SSSR 318, 1340–1344, (in Russian).

Kubotera, A., 1974. Volcanic tremors at Aso Volcano. In: Phys. Volcanol.. Elsevier, Amsterdam, pp. 29–48.

Lynnes, C.S., Thorne, L., 1989. Inversion of P coda for isotropic scatterers at the Yucca flat test site. Bull. Seismol. Soc. Am. 79, 790–804.

Matsumoto, S., 1996. Study of the inhomogeneous crustal structure around the Nikko area. PhD Thesis, Science, Tohoku University, Sendai, Japan, pp. 1–103 (in Japanese).

Matsumoto, S., Hasegawa, A., 1996. Distinct S wave reflector in midcrust beneath Nikko-Shirane Volcano in the northeastern Japan arc. Journal of Geophysical Research 101 B2, 3067–3083.

Mukhamedov, V.A., 1992. On fractal properties and generating mechanisms of high-frequency seismic noise. Izv. Akad. Nauk SSSR, Fiz. Zemli 3, 39–49, (in Russian).

Nikolaev, A.V., Troitskiy, P.A., 1987. Lithospheric studies based on array analysis of P-coda and microseisms. Tectonophysics 140, 103–113.

Nikolaev, A.V., Troitskiy, P.A., Tchebotareva, I.I., 1986. Dokl. Akad. Nauk SSSR 286, 586–591, (in Russian).

Nikolaev, A.V., Troitskiy, P.A., Tchebotareva, I.I., 1991. Analysis of Seismic Holography. VINITI, Moscow, N 18-B91, 52 pp. (in Russian).

Omer, G.C., 1950. Volcanic tremor. Bull. Seismol. Soc. Am. 40, 175–194.

Omori, F., 1911. The Usu-San eruption and earthquake elevation phenomena. Bill. Imp. Earth Invest. Comm., Tokyo 5, 1–38.

Rykunov, L.N., Khavrishkin, O.B., Tsyplakov, V.V., 1979. Temporal variations of high-frequency seismic noises. Izv. Akad. Nauk SSSR, Fiz. Zemli 11, 72–77.

Rykunov, L.N., Khavrishkin, O.B., Tsyplakov, V.V., 1980. Lunar–solar tidal periodicity in lines of spectra of temporal variations of high-frequency microseisms. Dokl. Akad. Nauk SSSR 252, 577–580, (in Russian).

Rykunov, L.N., Smirnov, V.B., Starovoit, Ju.O., 1986. On hierarchy character of the seismic emission. Dokl. Akad. Nauk SSSR 288, 81–85, (in Russian).

Rykunov, L.N., Smirnov, V.B., Starovoit, Ju.O., Chubarov, O.S., 1987. Self-similarity of the seismic emission in time. Dokl. Akad. Nauk SSSR 297, 1337–1341, (in Russian).

Rykunov, L.N., Starovoit, Ju.O., Khavrishkin, O.B., Tsyplakov, V.V., 1982. Connection of storm microseisms and high-frequency noises. Izv. Akad. Nauk SSSR, Fiz. Zemli 2, 88–91, (in Russian).

Sakai, S., 1994. Crustal structure beneath the high dense array. Program Abstr. Jpn. Seismol. Soc. 2 (D05), 291.

Sakuma, S., 1957. Volcanic tremor of Me'anan-dake. J. Fac. Sci., Hokkaido Univ. 1, 37–53, Ser. VII.

Sassa, K., 1935. Volcanic micro-tremors and eruption-earthquakes. Mem. Coll. Sci., Kyoto Univ. 18, 255–294.

Seidl, D., Schick, R., Riuscetti, M., 1981. Volcanic tremors at Etna: a model for hydraulic origin. Bull. Volcanol. 44, 43–56.

Shima, M., 1960. Volcanic microtremors at Volcano Aso. J. Phys. Earth 8, 1–17.

Smirnov, V.B., Cherepantsev, A.S., 1991. Relation between high-frequency seismic noise parameters and the dynamics of geophysical medium. Volcanol. Seismol. 5, 69–83, (in Russian).

Taner, F., Neidell, N.S., 1971. Semblance and other coherency measures for multichannel data. Geophysica 36, 482–497.

Tchebotareva, I.I., Nikolaev, A.V., Sato, H., Shiomi, K., 1997. A source of seismic emission related to a magma-body at the volcanic front on Honshu Island, Japan. Volcanol. Seismol. 2, 58–73, (in Russian).

Tokarev, P.I., 1981. Volcanic tremor. Volcanol. Seismol. 3, 55–72, (in Russian).

Tsumura, N., 1994. 3-D attenuation structure beneath the NE Japan arc based on the simultaneous determination of source parameters and *Q* values. PhD Thesis, Science, Tohoku University, Sendai, Japan, pp. 1–134 (in Japanese).

Yoshimoto, K., Sato, H., Kinoshita, S., Ohtake, M., 1993. High-frequency site-effect of hard rocks at Ashio, Central Japan. J. Phys. Earth 41, 327–335.

Zhadin, V.V., 1971. On the frequency composition of records of compression waves from distant earthquakes. Izv. Akad. Nauk SSSR, Fiz. Zemli 5, 99–101, (in Russian).